

On The Atmospheres of Objects in the Kuiper Belt

S. Alan Stern

**Space Science and Engineering Division
Southwest Research Institute
1050 Walnut Street, Suite 400
Boulder, CO 80302
astern@swri.edu**

and

**Laurence M. Trafton
Department of Astronomy
University of Texas
Austin, TX 78712
lmt@astro.as.utexas.edu**

22 February 2007

**Submitted to the Space Science Series Volume
“Kuiper Belt Objects”**

Abstract

Atmospheres around solar system bodies reveal key insights into the origins, chemistry, thermal evolution, and surface/interior interaction of their parent bodies. Atmospheres are also themselves of intrinsic interest for understanding the physics and chemistry of gaseous envelopes. Furthermore, atmospheres also reveal information about primordial nebular materials trapped in accreting bodies. For these reasons and others, the detection and study of atmospheres on objects in the Kuiper Belt (KB) is of interest. Here we review what is known about the atmosphere of both KBOs and planet Pluto; we then go on to more generally examine the source and loss processes relevant to KBO atmospheres, the likely kinds of vertical and horizontal structure of such atmospheres, and then briefly reflect on KBO atmospheric detection techniques.

1. Motivation

In our solar system, atmospheres range from the tenuous, Surface Boundary Exosphere (SBE) of the Moon, Mercury, icy satellites and asteroids (e.g., *Stern*, 1999) to the freely escaping, collisionally thick atmospheres of comets, to the classical atmospheres of Mars, Venus, Earth, Titan, and the giant planets.

We set the stage for this review chapter by considering the requirements for atmospheric generation on KB bodies, which are simple: All that is required is the presence of gases or sublimating/evaporating materials on, or sufficiently near, the surface, and a source of energy that can maintain substantial vapor pressures generated from the available reservoir of volatiles.

For atmospheres to persist over geologic time there is an additional requirement that the loss of volatiles be less than complete by the present epoch. So in the case of low-gravity bodies like Kuiper Belt Objects (KBOs), which we will show to have prodigious atmospheric escape rates, this in turn implies some re-supply mechanism to the surface, such as internal activity, or the import or up-dredging of volatiles from impactors.

Atmospheres can be very generally defined to include both gravitationally unbound gaseous envelopes such as exospheres, or unbound cometary comae, as well as gravitationally bound collisional ensembles of gas. An exosphere is the portion of an atmosphere that is sufficiently rarefied that it escapes directly to space by one or more processes; i.e., it is the portion of an atmosphere where the mean free path exceeds the density scale height, so that molecules with sufficient energy can be expected to escape directly to space.

In atmospheres which are too rarefied to have anything but an exosphere, their gases escape at the speed of sound, and the atmospheric density falls off as $1/r^2$.

In what follows we discuss the likelihood and characteristics of what one expects for KBO atmospheres. We begin in §2 with a concise overview of evidence for atmospheres around KBOs, and Centaurs (inward scattered KBOs). We then proceed in §3 to give a very brief overview of what is

known about Pluto's atmosphere—the only presently established atmosphere around a bona fide KBO. In §4 we discuss production mechanisms for atmospheres in the KB region. In §5 we then describe atmospheric loss processes. We follow that with a discussion of expected KBO atmospheric vertical and horizontal structure in §6. We conclude in §7 with a brief look at future KBO/Centaur atmospheric detection and study prospects.

2. KBO Atmospheric Detections and Related Evidence

In the Kuiper Belt region, only one body is presently known to have an extant atmosphere: Pluto (though Neptune's moon Triton has an atmosphere and almost certainly had some former relation to the Kuiper Belt).

Perhaps foreshadowing the eventual discovery of the KBO atmospheres we will discuss below, the existence of Pluto's atmosphere was speculated about long before it was observationally established. Early arguments for an atmosphere around Pluto were based entirely on theoretical considerations (e.g., *Hart, 1974; Golitsyn, 1975*), but these were supplanted by strong circumstantial evidence for a vapor pressure equilibrium atmosphere after the discovery of the volatile CH₄ ice on Pluto's surface (*Cruikshank et al., 1976; Stern et al. 1988*). The actual detection of Pluto's atmosphere only occurred later, when rare but formally diagnostic stellar occultations revealed the unmistakable signature of atmospheric refraction at roughly microbar pressure levels (*Hubbard et al., 1988; Elliot et al., 1989; Brosch, 1995*).

At Pluto, where the surface temperature varies from ~35 K in volatile rich regions cooled by latent heat sinks, to ~55 K in volatile free regions warmed to their pure radiative equilibrium temperature (e.g., *Stern et al 1993; Jewitt, 1994*), candidate volatiles that may comprise parent species in the atmosphere include Ne, Ar, O₂, CO, N₂, and CH₄ (*Stern, 1981; Stern and Trafton, 1984*). H₂ and He easily escape Pluto, and are therefore not expected to remain in sufficient quantity to be important at the present day, approximately 4+ Gyr after Pluto's formation. Heavy noble gases, like Kr and Xe, are volatile at the relevant temperatures for Pluto, but are so cosmogonically rare that they are not expected to be abundant in significant quantities (*Stern, 1981*). Of the species just reviewed, N₂, CO, and CH₄ have since been detected on Pluto's surface and must play significant roles in its

atmosphere. The same volatile species are likely to be important for other large worlds in the KB.

In the case of Pluto's large satellite, none of the volatiles mentioned just above have been discovered in its surface spectrum (*Grundy and Buie 2000*), so one might expect the prospects for an atmosphere at Charon to be dim. Consistent with this hypothesis, stellar occultations by Charon (e.g., *Elliot et al., 2003; Sicardy et al., 2003; Sicardy et al., 2006*) have failed to detect any atmospheric signature, with derived upper limits on the atmospheric pressure of 110 nbar for N₂ and 15 nbar for CH₄.

In contrast to the known atmosphere around Pluto, only upper limits have been placed on possible atmospheres around other KB bodies. To date, no published reports of stellar occultations of KBOs report atmospheric detections. Similarly, only negative results have been obtained in searches for light-scattering particulate comae.

Despite this, the discoveries of N₂, CH₄ and C₂H₆ (ethane) ices on the KBO 2005 FY9 (*Brown et al., 2006; Licandro et al., 2006*) and the tentative detection of N₂ and CH₄ on KBO Sedna and CH₄ on Eris (*Barucci et al., 2005; Licandro et al., 2006*) indicate that KBO atmospheres may be discovered in the future. And the report by *Hainaut et al. (2000)* that found a change in the light curve of KBO 1996 TO66 from a double peak to a single peak over the course of a year, which they suggested may have resulted from an episode of cometary activity, is of related interest.

Additional circumstantial evidence for atmospheres comes from the detections (see chapter by Brown et al. in this volume) of albedos of 60-90% for the large KBOs Eris, 2005 FY9, and 2003 EL61. Following the same logic that connected the detection of surface volatiles and a high albedo on Pluto to a strong case for an associated atmosphere, these clues strongly suggest that these KBOs have, or recently had, atmospheres. However, we stress that definitive evidence for atmospheres must come from occultations or direct spectroscopic detections of gas phase constituents—both of which are difficult. Model inferences alone, while suggestive, cannot be considered definitive.

We now turn to Centaurs, which are objects that have recently escaped from the KB to orbits among the giant planets, and therefore enjoy significantly increased insolation to drive ice sublimation. A variety of these objects have

shown activity at large heliocentric distances (e.g., 6 to 25 AU). In most cases, this activity manifests itself as an extended coma.

The first and most well-known case for atmospheric phenomena at a Centaur revolves around the Centaur 2060 Chiron. Chiron has long been known to exhibit both photometric variability (*Hartmann et al.*, 1990) and a sporadic cometary coma (*Meech and Belton*, 1989). Analysis of archival images reveal Chiron's activity as far back to the 1940s, and have shown that this activity occurs at all distances of its orbit, including near aphelion, with no clear correlation between the level of cometary activity and heliocentric distance (*Bus et al.*, 1991). Indeed Chiron was more active at its 1970 aphelion than it was near its 1989 perihelion.

What generates Chiron's atmospheric activity? *Bus et al.* (1991) detected CN in Chiron's coma, and *Womack and Stern* (1999) detected CO at low SNR. Large variability in the magnitude and timing of Chiron's outbursts and the observations of discrete jet-like features observed during a stellar occultation (*Elliot et al.* 1995) provide further clues. Together these various facts imply that Chiron's surface may contain an uneven distribution of surface or near-surface volatile ices, likely including CO, with both distributed and discrete surface sources of atmospheric gas and particulates. The variation in Chiron's activity with time may be related to a complex interaction between the sites of volatile frosts near the surface, obliquity effects, and heliocentric distance. Alternatively, it could be related to residual trapped heat at localized impact sites that can remain bottled up by low thermal conductivity for decades to centuries (*Capria et al.*, 2000). Similar phenomenology probably powers other active Centaurs with atmospheres.

Finally, it is worth noting that the captured dwarf planet Triton, now a satellite of Neptune, is known to possess an N₂-dominated atmosphere with some CH₄ and a base pressure not unlike Pluto's. Since Triton is also roughly Pluto's size and density, and is widely thought to have originated in the same region of the solar system as Pluto, it serves as a possible guide to future discoveries that may be made around dwarf planets in the KB and farther out as well.

3. Pluto's Atmosphere

In what follows, space limitations only allow us to provide an overview of what is known about Pluto's atmosphere. Our goal is to give an illustrative example of what might be anticipated regarding the nature and phenomenology expected in atmospheres that may later be discovered elsewhere in the KB. (Much more complete information about Pluto's atmosphere is contained in the suite of review articles published by *Yelle and Elliot 1997*, *Summers et al. 1997*, *Spencer et al. 1997*, and *Trafton et al. 1997* in the Space Science Series volume, *Pluto and Charon*).

As described in §2, despite earlier circumstantial arguments and the 1976 discovery of CH₄ frost on Pluto's surface, it was not until June 1988 that Pluto's atmosphere was definitively detected. This discovery was made by stellar occultation observations at eight separate sites in, around, and over Australia-New Zealand; see Figure 1. These various sites probed different chords across Pluto, showing that the atmosphere is global and exhibits a characteristic scale height H of 55.7 ± 4.5 km and a pressure of 2.3 μ bar at a distance of 1250 km from Pluto's center.

A CH₄ dominated atmosphere, corresponding to $\mu=16$ and an ~ 60 K upper atmospheric temperature was ruled out when both N₂ and CO were detected in high-quality IR spectra of Pluto on Pluto's surface in greater quantities than CH₄ (*Owen et al.*, 1993). For the assumption of $\mu=28$ (i.e., an N₂- or CO-dominated atmosphere), an upper atmospheric temperature near 102 K can be derived from these data, knowing that the scale height $H=kT/(m_p\mu g)$, where m_p is the mass of a proton, μ is the average molecular weight of the atmosphere, and T is its temperature and g is the local gravity.

The upper atmosphere probed by the 1988 occultation was modeled by an isothermal (102 ± 9 K) temperature structure above the nominal half-light radius of 1215 km from Pluto's center and a composition of pure CO or N₂ (e.g., *Yelle and Elliot*, 1997). A near-surface thermal gradient of 10-30 K/km was predicted to link the surface temperature to the upper atmosphere. *Yelle and Lunine* (1989) realized that CH₄ can act as a thermostat in Pluto's upper atmosphere by absorbing energy in the ν_3 band at 3.3 μ m, cooling via the ν_4 band at 7.6 μ m, and conducting heat to the surface, thus potentially explaining the high temperatures at the microbar pressure level in light of Pluto's colder (35-55 K) surface temperatures. *Strobel et al.* (1996) later showed that most of this heating (80%) actually occurs in the CH₄ band at

2.3 μm . For this “CH₄-thermostat” model to work, however, there must be sufficient quantities ($\sim 0.1\text{-}1\%$) of atmospheric CH₄.¹

The direct spectroscopic detection of gaseous CH₄ in Pluto’s atmosphere was finally obtained from high-resolution IR spectroscopy in 1994 (*Young et al.*, 1997). These workers found that the partial pressure of CH₄ was too high for methane in solid solution with nitrogen, but consistent with methane in vapor pressure equilibrium with pure CH₄ frost at 41 K to 45 K, as shown in Figure 2. This work also confirmed the T/μ finding from the 1988 occultation datasets that either CO or N₂ must dominate Pluto’s atmospheric composition and that gaseous CH₄ is only a minor constituent compared to the total, with a mole fraction of perhaps 1-9%. Despite being only a minor constituent, Pluto’s CH₄ abundance is clearly sufficient to make the CH₄-thermostat work.

Importantly, the 1988 stellar occultation light curves exhibit a sharp change of slope, or ‘knee’ during immersion and emersion ((*Hubbard et al.*, 1988; *Elliot et al.*, 1989); see also Figure 1). The change in slope of these light curves below the half-light level indicates either non-isothermal temperature structure in the atmosphere (which changes the refractive index; e.g., *Eshelman* 1989; *Hubbard et al.*, 1990; *Stansberry et al.*, 1994) or an extinguishing photochemical haze layer (*Elliot et al.*, 1989), or both.

Extrapolations of the 1988 occultation light curves to the surface depend on the assumed radius of Pluto. Pluto’s radius is uncertain to approximately $\pm 3\%$, so the surface pressure and atmospheric column are also both uncertain. Pluto’s radius values are constrained by both an uncertainty in interpreting the stellar occultation data, which may not probe to the surface, and an uncertainty in the surface ice temperature, which is constrained but not fixed by the vapor pressure of N₂. The various constraints suggest bracketing radii and surface pressures, respectively, of 1200 km and 3 microbar and 1145 km and 28 microbar (e.g., *Spencer et al.*, 1997). The corresponding Pluto atmospheric column densities are 39 and 285 cm-am, respectively. Further, both hazes and refractive effects (e.g., mirages; *Stansberry et al.*, 1994) introduce considerable (10-30 km) uncertainties in radius determinations. These and other effects in turn create significant

¹ It is worth noting that this model does not work for Triton, at least without some modifications as discussed by *Elliot et al.* (2000). CO plays an important role in cooling these atmospheres by rotational line emission as was shown for Pluto (*Strobel et al.*, 1996) and Triton (*Elliot et al.*, 2000). This will be discussed further in §5.

uncertainties in resulting estimates of the surface pressure, with plausible values ranging from ~ 2 to perhaps ~ 60 μbar . As an aside, assuming complete atmospheric condensation near aphelion, this range of surface pressure corresponds to a seasonally deposited pure N_2 frost layer that would have a depth on the surface of 0.5 to perhaps 10 mm, depending on the actual base pressure and the frost porosity.

Stellar occultations by Pluto are rare, and no subsequent event was observed until August 2002. From that well observed event it was found that Pluto's atmospheric pressure had significantly increased from 1988 (*Elliot et al.*, 2003; *Sicardy et al.*, 2003). This pressure increase—a full factor of two—was initially surprising to some, since Pluto had been receding from the Sun as it moved away from its 1989 perihelion. However, the observed factor of two pressure doubling only requires an increase in N_2 surface frost temperature of 1.3 K (*Elliot et al.*, 2003), which could be the result of a thermal phase lag following Pluto's 1989 perihelion maximum in insolation (e.g., *Stern et al* 1988; *Trafton*, 1990; see also the review by *Spencer et al.*, 1997). It can also be explained by the exposure of new, volatile-rich terrains to sunlight as the southern (IAU convention) polar cap moved into summer, or a combination of both effects.

In addition to the increase in atmospheric pressure, a notable increase in the number of strong refractive spikes was also observed in the occultation light curves of 2002 compared with 1988 (e.g., *Pasachoff et al.*, 2005); this has been associated with an increase of turbulence or waves in Pluto's atmosphere. And yet another important change seen from 1988 to 2002 was the dramatic muting of the kink in the occultation light curves seen near the half light level in 1988. This indicated that a change in the atmosphere's vertical structure had also taken place. Together these various findings make clear that Pluto's atmosphere is time variable, likely due to a combination of seasonal and heliocentric distance effects.

One final result from the 2002 event is worth mentioning here. *Elliot et al.* (2003) reported that observations at a variety of wavelengths from $0.75 \mu\text{m}$ to $2.2 \mu\text{m}$, showed that the minimum flux of the light curve varies with wavelength, indicating that there is extinction in Pluto's lower atmosphere. While this does not rule out a thermal gradient also being in effect, it is clear evidence for a haze layer.

An even more recent stellar occultation of Pluto was observed at several sites on 12 June 2006. Data analysis is currently in progress, but initial results reveal that the 2006 atmospheric pressure and temperature structure in 2006 is far more similar to what was observed in the 2002 occultation (see Figure 3), than to 1988. Given the much shorter time base (four years vs. fourteen), this is not particularly surprising, but it is nonetheless noteworthy that the pace of change was not further accelerating.

Regarding orbital and seasonal change on Pluto, dramatic atmospheric change on Pluto was predicted as early as the beginning of the 1980s (*Stern, 1981; Trafton and Stern, 1983*) because Pluto's surface sees large changes in insolation and insolation distribution during its orbit around the Sun. These are due to both its large variation in heliocentric distance (29.5 to 49.6 AU) and its high (~120 deg) axial obliquity. Such insolation changes result in surface temperature variations that probably drive strong vapor pressure variations, in turn resulting in the transport of ices across the surface on seasonal and orbital timescales.

Unfortunately, quantitative models of Pluto's so-called "seasonal change," though adequately sophisticated, are not well constrained because numerous model input parameters (e.g., the compositional distribution, the albedo distribution, the surface temperature distribution, the thermal inertia) are not adequately known. Various models predict differing atmospheric pressure and volatile transport histories, and suggest that Pluto's surface/atmosphere interactions are more dramatic than any planet or satellite that orbits closer to the Sun, except perhaps Triton. And predictions of the timing and degree of post-perihelion atmospheric collapse (i.e., a factor of >100 decline in mass) as a condensation frost onto the surface vary widely (e.g., *Stern et al., 1988; Yelle and Lunine, 1989; Trafton 1990; Hansen and Paige, 1996; Lykawka and Mukai, 2005; see also Spencer et al., 1997* for a review). Why? The process of atmospheric collapse is complicated by both the patchy nature of Pluto's volatile distribution and thermal emission, as well as the complex, non-linear feedbacks that volatile transport drives on atmospheric and surface properties, and ultimately, the volatile distribution itself (e.g., *Spencer et al., 1997; Trafton et al., 1997*). It is likely that good atmospheric collapse (and subsequent regeneration as Pluto next approaches perihelion) predictions will require the surface albedo, temperature, and composition maps that NASA's New Horizons Pluto flyby mission will deliver in 2015. Whether the atmosphere is extant at that time, however, is not clear.

We now conclude this section by briefly considering the escape of gases from Pluto's atmosphere as a precursor to a more general discussion relating to KBO atmospheric escape in §5.

Pluto's combination of low surface gravity ($\sim 55 \text{ cm/s}^2$) and comparatively high stratospheric temperature ($\sim 100 \text{ K}$) conspire to create a circumstance where a much greater fraction of the initially Maxwellian distribution of molecular energies is capable of escape than in a typical planetary atmosphere. Indeed, unlike the terrestrial and giant planets and Triton, where Jeans escape and photochemical/ion pickup processes dominate, on Pluto, the hydrodynamic (i.e., streaming, bulk) escape of atoms and molecules likely dominates (e.g., *Trafton et al.*, 1997 and references therein).

Hunten and Watson (1982) (hereinafter HW82), pointed out that hydrodynamic escape of Pluto is energy-throttled by the adiabatic cooling of the expanding atmosphere, which is regulated by the downward conduction of solar FUV/EUV heat absorbed in the thermosphere. The HW82 formulation provides an upper limit to the escape flux because it approximates the sub-thermosphere temperature minimum to be 0 K.

Other investigators have used related methods to estimate escape rates for Pluto at perihelion, finding rates between $3 \times 10^{26} \text{ s}^{-1}$ and $2 \times 10^{28} \text{ s}^{-1}$ (*McNutt*, 1989; *Hubbard et al.*, 1990; *Trafton et al.*, 1989, 1997). All are upper limits except for Trafton, who solved the hydrostatic escape equations for a CH_4 atmosphere, estimating $3.3 \times 10^{27} \text{ s}^{-1}$. *McNutt* (1989) first considered a gas other than CH_4 (namely, CO) in hydrodynamic escape, using a self-consistent analytic approach. *Yelle* (1993) presented numerical solutions of the Navier-Stokes equations for Pluto's hydrodynamically escaping atmosphere for N_2 and CO that included solar EUV heating, energy transport by thermal conduction, and viscous dissipation of mechanical energy. *Krasnopolsky* (1999) extended McNutt's analytic approach to include a neglected term in the hydrodynamic flow equations; and he also included the hitherto neglected solar UV heating of Pluto's upper atmosphere, which he showed to be 6 times stronger than the solar EUV heating. He then applied these results to the hydrodynamic escape of Pluto's N_2 , with CH_4 diffusing upward through it, deriving a perihelion N_2 escape rate of $2.3 \times 10^{27} \text{ s}^{-1}$ at mean solar activity. Recently, *Tian and Toon* (2005) were the first to solve the time-dependent hydrodynamic escape equations for a planetary atmosphere and to apply them to the hydrodynamic escape of N_2 from Pluto, treating the spatial distribution of UV-EUV energy deposition realistically

over a range of depths in the atmosphere. They derived a corresponding perihelion escape rate around $1 \times 10^{28} \text{ s}^{-1}$, about an order of magnitude higher than the Krasnopolsky value. They argue that this discrepancy arises from Krasnopolsky's single-altitude heating approximation. This has merit in a case where the effective atmospheric depth of UV absorption is significantly lower than that of EUV absorption.

As we noted above, characteristic escape fluxes at perihelion of 3×10^{26} to $2 \times 10^{28} \text{ N}_2 \text{ sec}^{-1}$ have been predicted by various modelers. Over the 4.5 Gyr sec age of the solar system, this corresponds to the potential loss of 1 km to perhaps 10 km of surface ice, depending again in part on the surface ice porosity. This in turn implies either (i) an essentially 100% pure, volatile crust devoid of involatile constituents that would create, even in tiny amounts, a lag deposit that chokes off sublimation and therefore prevents atmospheric regeneration over time, (ii) a very recent source of surface volatiles and therefore atmosphere, or (iii) some kind of endogenic (e.g., geologic) or exogenic (cratering) activity that replenishes the source of volatiles available to the surface. Such considerations also apply to many KBOs, which may someday be discovered to have past or extant atmospheres which suffer similarly high escape rates.

4. KBO Atmospheric Production

We now turn to the subject of atmospheric generation on KBOs. In §5 and §6, respectively, we will discuss KBO atmospheric loss mechanisms and then structure. Three important atmospheric generation processes will be discussed here: ice sublimation, internal outgassing, and impacts. We take each in turn.

Ice Sublimation. Sublimation is the change of phase of a substance from the solid directly into the gaseous state. Sublimation is responsible for generating the atmosphere of Pluto, Triton, and comets.

Sublimation is an endothermic process: energy input is required to supply the latent heat of sublimation. In general, the kinetic energy of the molecules in the solid will have a distribution due to thermal or lattice motions. As a result, some fraction of the molecules near the surface will always have enough kinetic energy to overcome the binding potential energy of the lattice and escape into the gas phase, even though the temperature is below freezing. If the system is allowed to come to thermal equilibrium, then the rate at which gas molecules stick to the surface will equal the rate at which they "evaporate" from the surface, and the net latent heat transfer will be zero.

The equilibrium vapor pressure of any given frost is exponentially sensitive to the ratio of binding energy of the molecular matrix L , called the latent heat of sublimation, to its thermal energy kT ; this requires the condition that the gas density be high enough for the sticking rate to match the evaporation rate. Each of these rates is proportional to $e^{-L/kT}$, as is the equilibrium vapor pressure. In the case of more volatile frosts like N_2 , CO , and CH_4 , which are seen on Pluto, Triton, and some KBOs, L/k is such that an increase in temperature of only a couple of degrees K is enough to double the vapor-pressure.

Sublimation of an ice layer into a vacuum is a rapid, non-equilibrium process. The net evaporation flux (i.e., the difference between the sublimation and condensation rates of the gas) will cause the ice to cool (or heat, if the evaporation flux is negative). In the absence of other heat

sources, an upper limit on the rate of sublimation is set by the absorbed insolation.

When there are volatile ices of different species on the surface, the vapor pressures of their gas phase depend on how intimately they are mixed (see *Trafton et al.*, 1997). If they exist separately or as a mixture of their pure grains, then each ice's vapor pressure is specified by its temperature according to the saturation vapor pressure relation for that ice. When two or more volatile ices are mixed together intimately as in a solid solution, the less volatile ice will become enriched at the surface as the more volatile ice preferentially sublimates. From a surface evolution standpoint, this can eventually reduce the sublimation rate of the surface to that of the less volatile ice. Differential sublimation will be controlled by Raoult's Law, and if any refractory impurity exists in an ice, then an involatile lag deposit will form from impurities that cannot sublime (e.g., *Stern*, 1989). Even ice mixtures with impurities of 1% can be sufficient to create a lag deposit which will eventually choke off sublimation by burying the ice beneath an involatile overburden.

In the 30-50 AU KB zone, a rapidly rotating body warmed only by the Sun, with spin axis normal to the direction to the Sun and unit emissivity ϵ will have an effective temperature between 39 K to 51 K, or 31 K to 40 K, for bolometric albedos of 0 and 0.6, respectively. For either a slow rotator, or a fast or slow rotator with spin axis pointed towards the Sun, the mean dayside effective temperature would be some 8-10 K, higher. If $\epsilon < 1$, then the physical temperature would be higher than the above values by a factor of $1/\epsilon^{1/4}$. In the extreme, surface temperatures warmed only by insolation might reach ~ 70 K on KBOs. Tidal heating, radioactive decay, and other energy sources can further raise these temperatures, but volatile ices such as O_2 , N_2 , CO , and CH_4 already have significant vapor pressures in the 30-70 K temperature range. As a result, gaseous envelopes can accompany KBOs having volatile reservoirs in contact with the insolation field. The bulk atmospheric composition in such cases can be expected to reflect that of the illuminated reservoir ice, as it does for comets.

The saturation vapor pressures for three of these ices are shown in Figure 4 over a temperature range relevant to much of the Kuiper belt. Over this range the vapor pressures change dramatically, i.e., by 5-7 orders of magnitude. The diurnally averaged insolation and resulting surface temperature vary with latitude. Consequently, atmospheric vapor pressure

and density can vary dramatically over the surface for an atmosphere too tenuous to be in hydrostatic equilibrium (*Stern and Trafton, 1984; Trafton, 1990*).

Additionally, for KBOs having eccentric orbits, an orbital effect will result from the change in planetary-averaged insolation over the orbit, which in general will not be in phase with obliquity-driven seasons, although both will have the annual period. As a result, many KBOs with atmospheres are likely to have highly time-variable atmospheric bulk, composition, and structure.

Internal Outgassing. Outgassing from the interior is another important process, not only owing to the high volatile content of KBOs, but also because they may be unusually porous (see the chapter by *McKinnon et al.*). Such porosity increases the conductivity of volatiles to the surface and therefore the effective size of the reservoir that supports an escaping atmosphere or coma. The importance of internal release, whether from the near surface (as for Triton's geysers) or from deeper, cannot be underestimated since without a resupply of volatiles, an impure surface will eventually choke itself off as an ever-increasing thickness of involatile lag deposit accumulates.

To better understand interior evolution, *McKinnon (2002)* and *Choi et al. (2002)* conducted studies of the thermal evolution of KBOs of various sizes up to 500 km in diameter. *Choi et al. (2002)* found that the long-term evolution of the temperature profile and the structural modifications are a strong function of the KBO's accretion time, size, and dust/ice mass fraction rather than its heliocentric distance. Based on their 1-D, 10-500 km models with an initial composition of a porous mixture of H₂O, CO, and CO₂ ices and dust, and at distances of 30-120 AU, they expect CO, as well as N₂, and possibly CH₄, to be lost entirely. In contrast, the less volatile ices CO₂, H₂CO, and NH₃ should be partially retained. Other important thermal benchmarks include the temperature 155 K, where a eutectic CH₃OH-H₂O melt can form, and 190 K, which is sufficient to melt ice mixtures such as H₂O-NH₃, which would be buoyant and make its way upward.

Choi et al.'s calculations also show that the central temperature of a 100 km radius KBO may reach temperatures up to 180 K, and that the internal heating can result in a compositionally layered (differentiated) structure, with interlaced layers depleted and enriched in volatiles. For 150 km KBOs,

McKinnon (2002) found the central temperature limit to be only 105 K, but for a 450 km radius KBO, central temperatures can exceed 270 K, which opens the possibility of liquid H₂O in large KBOs and Pluto.

In this regard, cryogenic volcanism has been suggested to resurface Quaoar in response to the reported detection of crystalline water ice and possibly ammonia hydrate as well, both of which should have been destroyed by energetic particle irradiation on a time scale of ten million years unless recently resupplied (*Jewitt and Luu, 2004*). The reported crystallinity also indicates that the surface ice on Quaoar has been heated to at least 110 K.

Collisions. Objects in the KB have characteristic mutual collisional speeds of 1-1.5 km s⁻¹. As such, collisions represent both a source of energy to drive sublimation. The role of collisions was investigated by *Orosei et al. (2001)* who found that in some cases, depths over 1 km were altered by KBO impacts while for some other collisions, very small effects were produced. *Durda and Stern (2000)* found that over the 3.5 Gyr age of the classical Kuiper belt, impacts of 1-km radius comets onto individual 100-km radius KBOs occur some ~8-54 times, producing craters ~6 km in diameter.

By excavating deeply buried materials that are beyond the influence of solar heating, these collisions also have the potential to replenish surface ice previously depleted through escape or buried under a refractory lag deposit (*Stern 1989*). For example, a nitrogen ice deposit excavated from a 6 km diameter crater 1 km deep (presumably with an involatile material just above it) would correspond to a column abundance of 23 g cm⁻², or 180 m-am of gas on a 100 km radius KBO.

Additionally, impacts import energy and can either promptly or over time (depending on the impact speed and the depth of burial of the impactor) power the sublimation of volatiles at the impact site. At the 1-1.5 km s⁻¹ impact speeds characteristic of KBO collisions, H₂O is not promptly vaporized in large quantities. As for more volatile ices like N₂, CH₄, and CO, it is unfortunate that neither experiments nor adequate thermo-physical modeling has been undertaken (*E. Pierazzo, pers. comm.*), so it is not presently possible to quantify the efficacy of this process.

5. KBO Atmospheric Escape

Escape, as opposed to chemical destruction, is expected to be the dominant long-term loss process for atmospheres on KBOs. Unlike the cyclic effects of seasonal/orbital collapse of an atmosphere, escape results in the permanent loss of volatiles.

The escape rate from a KBO depends on both upper atmospheric density and temperature. The former controls the altitude of solar UV heating and the escape level; the latter controls the escape energetics. Because of the low escape speed of KBOs, typically 0.05 km/sec to 1.2 km/sec (corresponding to KBO radii of 50 km and 1270 km, respectively, for a reference density of 1.6 g cm^{-3}), their gas envelopes are likely to be predominantly escaping hydrodynamically. This means that a significant fraction of the Maxwellian is sufficiently energetic to escape, rather than just the high energy tail as in more classical, Jeans escape. This is illustrated by the fact that the mean thermal speed of N_2 at 20 K is 0.12 km s^{-1} , which is comparable to the escape speed from a KBO of radius 125 km having a density of 1.6 g cm^{-3} .

To illustrate this point further, a good general measure of the degree of boundedness of an atmosphere is the ratio of the gravitational potential of a molecule near the surface to kT . This dimensionless gravitational parameter is

$$\lambda = GMm_p\mu/RkT. \quad (1)$$

Here G is the universal gravitational constant, M is the KBO's mass, m_p is the mass of a proton, μ is the mean molecular weight of the atmosphere, R is the KBO's effective radius, and T the exospheric temperature.

An atmosphere with $\lambda=2$ is hardly bound since it blows off (escapes hydrodynamically) at sonic speed. Over the range $3 < \lambda < 140$ that is expected on larger KBOs, atmospheric escape is likely to span the short atmospheric lifetime hydrodynamic streaming regime to the long atmospheric lifetime thermal escape regime.

Evaluating the constants in the above equation, we obtain the dimensionless relation:

$$\lambda = 3.361 \times 10^{-5} \mu \rho R^2 / T, \quad (2)$$

where density ρ replaces M assuming a homogeneous sphere of radius R in kilometers. In Table 1 we provide the surface value of λ as a function of KBO size, assuming N_2 -, CO -, and CH_4 -dominated atmospheres, an exospheric temperature range of 25-100 K, and $\rho=1.6 \text{ g cm}^{-3}$.

Table 1
 λ Estimates for KBOs Having CH_4 -, CO -, or CH_4 -Dominated Atmospheres

Radius (km)	μ	λ range (over $T=25\text{-}100 \text{ K}$)
250	16	0.6 - 2.2
250	28	1.0 - 3.8
500	16	2.2 - 8.6
500	28	3.6 - 15
1000	16	16 - 32
1000	28	16 - 60
1500	16	20 - 78
1500	28	34 - 137

Here $\mu=16$ represents a CH_4 -dominated atmosphere and $\mu=28$ represents an N_2 or CO -dominated atmosphere.

We now discuss in turn the various modes of gravitational escape that KBO atmospheres can be expected to experience, based on their individual λ 's and atmospheric structure.

Jeans Thermal Escape. The lowest escape rates occur for atmospheres that are in the Jeans escape regime, where escape occurs by molecular evaporation of the Maxwellian high-velocity tail. Jeans escape is limited by the energy input available to heat the exosphere. This thermal escape takes place from an exobase, the altitude where the mean free path equals the local scale height. Jeans escape is limited by the energy input available to heat the exosphere.

Jeans escape must take place near the planet because as the atmospheric temperature rises, or as λ otherwise becomes smaller, the exobase altitude rises towards $\lambda=2$, while the escape transitions to the hydrodynamic regime

(see below) as the gravitational binding energy of the gas molecules declines to approach the mean thermal kinetic energy.

It is important to note that Jeans escape, in effect, cools the exosphere by removing its highest velocity molecules and atoms. As a result, the velocity distribution of the exosphere—the region above the exobase—will deviate from a strict Maxwellian and the escape rate will drop below the classical Jeans value if the escape rate is too high for atmospheric diffusion to readily replace the higher-energy escaping molecules. One must therefore be careful in calculating Jeans escape rates to properly account for this and other effects that modify the bulk gas temperature, and hence kT .

The Jeans escape flux at the exobase is given by:

$$F_e = n_e U (1 + \lambda_e) \exp(-\lambda_e) / (2 \sqrt{\pi}). \quad (3)$$

Here $U = (2kT_e/m)^{1/2}$, m is the mass of the escaping molecular species of interest, and T_e , n_e , λ_e , are the temperature, number density, and gravitational parameter, respectively, at the exobase. One thus sees that the Jeans escape rate is highly sensitive to the value of λ at the exobase, decreasing exponentially with it.

The Jeans escape regime typically obtains for atmospheres around massive planets, where it results in very low escape rates. In fact, the Jeans escape timescale of such planetary atmospheres can be longer than the age of the solar system.

Atmospheres in the Jeans escape regime are unlikely to occur on most KBOs, owing to the low mass of most KBOs. However, depending on the composition (hence μ), Jeans escape could dominate on Pluto/Triton-sized or larger KBOs.

As an example of one type of KBO atmosphere that may be encountered, Triton's atmosphere is entirely in the Jeans regime, including the escape of H, H₂, and N generated by CH₄ photolysis and ion chemistry driven by precipitating electrons trapped in Neptune's magnetosphere (*Summers and Strobel, 1991; Krasnopolsky, 1993; Strobel et al, 1996*). For a Triton-like exobase height of 900 km and exobase temperature of 100 K, the escape-level $\lambda = 21.5$ and N₂ number density is $1.1 \times 10^7 \text{ cm}^{-3}$, according to the

preferred Triton model of *Krasnopolsky* (1993; his Table 9). In his basic models, the number density of N_2 is insensitive to the flux of magnetospheric electrons; the CO mixing ratio is 10^{-3} in his preferred model. The N_2 Jeans escape flux is only $2140 \text{ cm}^{-2} \text{ s}^{-1}$ or $5 \times 10^{20} \text{ s}^{-1}$, far below the hydrodynamic regime.

In closing, Jeans escape can occur for any value of λ at the exobase greater than ~ 2 . This escape regime is most likely for cold, high molecular-weight atmospheres around dense, massive bodies. The loss of volatiles from small KBOs having lower λ values is likely to occur through the direct sublimation of volatile ice to space. The sublimation flux into a vacuum is then governed by the speed of sound for the escaping molecules and a molecular density that is constrained by the saturation vapor pressure.

Hydrodynamic Escape. As we stated above, hydrodynamic escape involves the wholesale escape of a large fraction of the bulk Maxwellian, it occurs when λ is very low. While Jeans escape is an evaporative process from an essentially static atmosphere, hydrodynamic escape is a collisional process that maintains a non-zero bulk outflow speed throughout the atmosphere.

This process may occur on KBOs having λ only a bit greater than 2 (e.g., 3-6), but it fails when escape is limited by a process other than energy deposition into a thermosphere. One example of this is an escaping KBO atmosphere that is optically thin to EUV radiation. It also fails when the absorbed insolation occurs over a wide range of altitudes, as may be the case when multiple gases are present with very different FUV/EUV absorption cross sections. Hydrodynamic escape may still occur in these situations, but its treatment requires a less-approximate solution of the escape equations.

When the hydrodynamic escape regime is achieved, it can be sub-classified according to whether the exobase of a secondary gas that is diffusing through a primary (i.e., hydrodynamically) escaping constituent, lies below or above the height at which the primary species becomes supersonic. Following *Krasnopolsky* (1999), one can distinguish between two hydrodynamic escape regimes, “slow” and “fast” hydrodynamic escape.

In slow hydrodynamic escape, the upwardly diffusing secondary gas escapes thermally from an exobase that lies below the sonic level of the primary, hydrodynamically escaping constituent. The hydrodynamic speed at the

exobase adds to the radial component of the speeds of the thermally escaping species. This occurs in the case of the minor constituent CH_4 in Pluto's atmosphere, which buoyantly diffuses upwards through the primary gas, N_2 . Since its exobase lies below the sonic level, it arrives at the exobase still having a quasi-thermal velocity distribution that is not wholly relegated to streamline flow. It thus escapes from this level quasi-thermally, with escape favoring the fastest molecules. This is opposite to classical hydrodynamic escape where the exobase lies above the sonic level, and the upward diffusing species fully participates in the bulk hydrodynamic escape.

In contrast, in the fast hydrostatic escape regime the thermal energy of all escaping species has been effectively converted through cooling collisions to streamlined, radial, transonic velocities with escape rate close to the UV-EUV solar energy input limit (*Hunten and Watson, 1982; Trafton et al., 1997*).

Application to KBOs. KBO atmospheres having large scale heights that are a significant fraction of the KBO radius have small λ values (as low as ~ 2), and so should exhibit hydrodynamic escape since they are gravitationally weakly bound. In contrast, KBO atmospheres with small scale heights that lie deep in the body's gravitational potential should be escaping thermally from an exobase. With an exobase λ of 21, Triton is such an example. The crossover escape flux between the two regimes depends on the value of λ and the mean thermal speed at the exobase, and the surface λ and amount of EUV heating, respectively. With $H=56$ km, $\lambda=22$ at the occultation level² (1250 km), and a CH_4 exobase lying below the sonic altitude, Pluto is an example of a KBO in the transition region between Jeans and hydrodynamic escape. However, it is also possible for KBOs to be in the transition region between Jeans and hydrodynamic escape.

An important factor in whether a given KBO atmosphere will be in the Jeans, transitional, or full hydrodynamic escape regime, is the atmospheric CO/CH_4 ratio. CO is a net coolant in thin, cold, vapor pressure-supported atmospheres that do not have large optical depths in the CO lines. In

²Notice this is the occultation level, not the exobase level, which is where λ was calculated for Triton above. Pluto is not at its exobase, but at the occultation level. Pluto's N_2 does not have an exobase. The regimes are different because Triton's atmosphere is evaporating slowly at the exobase, while Pluto's N_2 is escaping hydrodynamically, with a much higher flux. Hydrodynamic escape depends on the flux of solar UV-EUV heating of the thermosphere, as well as λ ; hence, equality of λ does not imply equality of escape regime.

contrast, when the optical depth of sunlight to CH₄ is high, CH₄ is a net heating source. The relative amounts of these gases therefore determine the radiative equilibrium temperature structure in such KBO atmospheric layers, and thus the density and scale height variation. For example, the surface CH₄ mixing ratio is two orders of magnitude higher for Pluto than for Triton, so CH₄ is primarily responsible for heating Pluto's low stratosphere to 100 K. Triton's lower CH₄ mixing ratio accounts for Triton's significantly colder atmosphere at the μ bar level (*Krasnopolsky 1993; Strobel et al., 1996*). Pluto's higher CH₄/CO ratio results in Pluto's higher temperature and larger scale height, and therefore its greater, hydrodynamic, escape rate.

6. KBO Atmospheric Structure

In this section we will discuss both the vertical and lateral structure of atmospheres one may find around KBOs.

The column abundance and base pressure of an ice-supported KBO atmosphere will depend sensitively on the ice temperature (through the saturation vapor pressure relations) and on the scale height. In the approximation of an isothermal atmosphere, the column abundance N of gas in cm-am units (1 cm-am is the number of molecules in 1 cm³ of gas at STP) is the product of the equilibrium vapor pressure of the ice $P_s(T)$, converted to density, and the atmospheric scale height corrected to first order for sphericity. Thus, the column is, in cm-am, is:

$$N = 10^5 P_s(273/T_{ice})(R/\lambda)(1+2/\lambda). \quad (4)$$

Here T_{ice} is the ice temperature, $P_s(T_{ice})$ is in bars, R is in km, and the dimensionless gravitational parameter λ is evaluated at the KBO's surface.

Table 2 below estimates the gas column N , and a range of other atmospheric parameters, for two KBO radii and various relevant surface temperatures; it assumes a KBO density of 1.6 g cm⁻³. The other parameters are the surface λ , scale height, and pressure. For the temperature and radius ranges listed, λ varies between 2.8 and 53, and H varies from 12 to 145 km. The surface pressure and column abundance estimates range over ten orders of magnitude. Higher values are expected on KBOs with polar illumination because their equilibrium temperatures will be higher, generating higher vapor pressures. The N values are least certain at the lowest λ value, where the scale height is an appreciable fraction of the KBO radius.

Table 2
KBO Atmospheric Characteristics

R (km)	T (K)	λ	H (km)	Pressure (μbar)	N (cm-am)
CH ₄ ($\mu=16$)					
400	32	4.3	93	5.0×10^{-6}	5.7×10^{-4}
400	50	2.8	145	2.9	402
1400	32	53	27	5.0×10^{-6}	1.2×10^{-4}
1400	60	28	50	153	3700
N ₂ ($\mu=28$)					
400	25	9.6	42	1.1×10^{-4}	5.8×10^{-3}
400	50	4.8	83	3960	$2.5 \times 10^{+5}$
1400	25	12	12	1.1×10^{-4}	1.4×10^{-3}
1400	60	49	29	6.3×10^4	$8.5 \times 10^{+5}$

Quantities refer to values at or near the surface. A KBO density of 1.6 g cm^{-3} is assumed.

With this information in hand, we now turn to the vertical structure considerations for KBO atmospheres.

Vertical Structure. The vertical structure of KBO atmospheres is most strongly affected by four primary kinds of physics: hydrostatic equilibrium, vapor pressure, atmospheric escape, and radiative transfer.

The pressure scale height $H=R/\lambda$ (same as the density scale height in an isothermal atmosphere) characterizes the atmospheric vertical pressure structure, which is determined by hydrostatic equilibrium or escape. For KBOs smaller than ~ 100 kilometers in radius, the scale height will usually exceed the KBOs radius, and even for KBOs as large as 500 kilometers in radius, scale heights will be a significant fraction of the KBO radius. As a result, atmospheres around all but the very largest KBOs are expected to have significant sphericity effects, making the plane parallel approximation inadequate.

Figure 5 shows pressure vs. altitude curves for simple isothermal KBO atmospheres for two bracketing sizes, temperatures, and compositions. The barometric approximation with hydrostatic equilibrium was assumed; so the curves do not account for the effects of atmospheric escape. A KBO density

of 1.6 g cm^{-3} and surface pressure of $15 \text{ } \mu\text{bar}$ was also assumed; curves for other surface pressures can be estimated by sliding the curves or pressure scale horizontally. The effect of molecular weight, temperature, and radius on the scale height is evident. Any KBO atmosphere can be expected to be quite extended, especially for CH_4 on a smaller KBO.

The thermal structure of a KBO atmosphere will depend on the distance from the Sun, on the atmospheric composition, on the internal radiative transfer, on adiabatic expansion and cooling due to escape, and on the balance between the atmospheric absorption of heat from the Sun plus surface, and the heat lost from net sublimation and radiation to space.

With atmospheric surface pressures expected in the μbar regime and lower, the atmospheric thermal opacity is too low to drive lower atmosphere convection. Sublimation winds that transport volatiles to lower-temperature regions of the globe will be most effective in the lowest scale height of the atmosphere. Just above this regime, the thermal structure will depend on whether the atmosphere experiences net heating at these levels.

Both CH_4 and CO have absorption bands capable of absorbing near-infrared sunlight and radiating it at longer wavelengths, which affects the temperature and density structure. In the case of CH_4 alone, this results in a net heating of the upper atmosphere. For a Pluto-like atmospheric pressure (μbars or tens thereof), a CH_4 mixing ratio of 1-2% is required to elevate a KBO thermospheric temperature to 100 K in $\sim 10 \text{ km}$ (*Yelle and Elliot, 1997*). To raise the temperature to 100 K but with a smaller temperature gradient, a mixing ratio of 0.1% is sufficient. N_2 gas does not have this ability. On the other hand, CO is a net coolant of KBO thermospheres via mm and sub-mm radiation (*Strobel et al., 1996*). Such cooling is more important than near-IR heating and could be sufficient to inhibit hydrodynamic escape if the CO/CH_4 mixing ratio is large enough, as is the case for Triton (see also §5).

For KBO atmospheres escaping in the hydrodynamic regime, the atmosphere cools adiabatically, which limits the escape rate. Escape will then be regulated by EUV+UV solar heating of the upper thermosphere, if one exists. Above these absorption levels, the exospheric temperature will peak, then drop off while the escape speed becomes transonic. The heat conducted downward from this level offsets the adiabatic cooling below to regulate the escape rate, much like a throttle. This causes a temperature

minimum in the lower atmosphere, which affects the density structure (*Hunten and Watson, 1982; Trafton et al. 1997; Tian and Toon, 2005*).

Lateral Structure and Conditions for Atmospheric Globality. An important point about the low pressure atmospheres expected around KBOs is that they may not in all cases be global. Instead, in some cases, local atmospheric “domes” may occur (e.g., over a subsolar region). Thus, globality is an important KBO atmospheric structural attribute.

Pluto has a thermal light curve (*Lellouch et al., 2000*), even though its volatile ice is expected to be globally isothermal, because the sublimating ices do not cover the surface uniformly. Thus, its thermal light curve arises because the non-volatile surface does not sublimate and therefore does not cool (e.g., *Stern et al., 1993; Spencer et al., 1997*). For a steady-state KBO atmosphere to be global, it must have sufficiently small lateral gradients. This in turn implies that the reservoir of sublimating surface ice must be globally isothermal (neglecting topographic elevation differences), even if the ice itself is not distributed globally.

Isothermality is achieved and maintained by “sublimation winds” created by the net sublimation of ice from regions of higher temperature or insolation to icy regions of lower temperature or insolation. This transfer of volatiles through the atmosphere is accompanied by a latent heat flux that effectively redistributes the ice-absorbed insolation heat evenly to all of the exposed volatile ices, which then radiates this heat away (*Trafton and Stern, 1983*). The resulting radiative balance, averaged over a diurnal cycle, determines the global ice temperature. For ice isothermality to occur, the mass of the atmosphere has to be high enough for the sublimation winds to transport sufficient latent heat flux to effect this redistribution at wind speeds low enough for the atmosphere to approximate hydrostatic equilibrium. This in turn sets a lower limit to the vapor pressure and temperature of the ices.

In quantitatively evaluating this criterion, we have followed the formalism given in the Appendix of *Trafton (1984)* that was applied to Triton to estimate the conditions under which a KBO atmosphere is supported hydrostatically on a global basis such that the volatile surface ice is isothermal. That work considered the net sublimation of ice covering Triton’s surface for two bracketing geometries: solar latitude 0 and 90 deg, and allowed for radiative losses and the polar insolation geometry. The insolation geometry is relevant because insolation over the equator generates

two sublimation winds, each moving polewards in opposite hemispheres while polar illumination generates a single wind moving towards the opposite pole. Atmospheric escape and its associated cooling are neglected in this model. Sublimation winds originating at low subsolar latitudes were assumed to travel to polar regions and freeze out. Sublimation winds originating in a polar region at high latitudinal insolation were assumed to travel to the opposite pole after reaching minimum speed and maximum density at the equator—the inverse solution. A necessary condition for globality was found to be that the equatorial sublimation wind speed v_0 must be small compared to the speed of sound $v_s=(\gamma kT/\mu m_p)^{1/2}$; here γ is the ratio of the specific heats of the gas.

This condition, that the speed of the sublimation wind must be adequately subsonic (see also *Trafton and Stern, 1983; Ingersoll, 1990; Trafton et al., 1997*), ensures that the accompanying latent heat flux is sufficient to redistribute the absorbed insolation in order to eliminate significant horizontal temperature and pressure gradients. In this circumstance, atmospheric structure has a high degree of symmetry and regularity, except for the sublimation wind itself, which is affected significantly by the subsolar latitude.

This regulation occurs for Pluto, Triton, and Mars, but does not occur for ices supporting an exosphere or a very thin collisional atmosphere, such as Io's, that is not close to overall hydrostatic equilibrium. Such thin atmospheres tend to be “patchy”; i.e., clustered around isolated volatile ice sublimation sources on the surface.

So what obtains on KBOs? Following *Trafton and Stern (1983)*, we adopt the criterion for a significant deviation from hydrostatic equilibrium of a KBO atmosphere to be a 10% drop in pressure going from the equator to colatitude 10 deg. Equation A6 of *Trafton and Stern (1983)* then gives $v_0=0.072v_s$. This wind speed leads one to the minimal column abundance for global hydrostatic equilibrium for the case of insolation-limited sublimation:

$$N_{\min} = \xi(30/r)^2(1-A)R/L(T_{\text{ice}})/(\gamma\mu T)^{1/2}. \quad (5)$$

Here, N_{\min} is in cm-am, r is the solar distance of the KBO in AU, A the surface albedo, R the radius in km, $L(T_{\text{ice}})$ the latent heat of sublimation of the ice in erg g⁻¹ (given along with the vapor pressures, e.g., in *Brown and*

Ziegler 1980)³, and T the lower-atmospheric temperature, approximated by the ice temperature. The constant $\xi=1.497 \times 10^8$ here for a subsolar latitude of 0 deg; and $\xi=1.459 \times 10^9$ for a subsolar latitude of 90 deg. Diurnal ice temperature variations are assumed negligible due to latent heat transfer.

Requiring equality of the two expressions for column abundance, i.e., $N=N_{\min}$ yields the limiting ice temperature T_{ice} for global hydrostatic equilibrium and surface ice isothermality. Sample values of N_{\min} for various solar distances are given in Tables 3 and 4 for some representative KBO parameters. Both the equatorial and polar insolation cases assume that the KBO is covered with volatile ice radiating heat uniformly to space.

Table 3
KBO Atmospheres for Equatorial Illumination¹

R (km)	A	r (AU)	T_{crit} (K)	λ	H (km)	Pressure (μbar)	N_{min} (cm-am)
CH₄ (μ=16)							
400	0.0	56.3	37.2	3.71	108	8.17×10^{-4}	0.099
400	0.6	35.6	37.2	3.71	108	8.26×10^{-4}	0.099
1400	0.0	45.3	41.4	40.7	34.4	2.14×10^{-2}	0.505
1400	0.6	28.6	41.2	40.7	34.4	2.17×10^{-2}	0.508
N₂ (μ=28)							
400	0.0	109	26.7	9.04	44.2	1.29×10^{-3}	0.052
400	0.6	69.1	26.7	9.04	44.2	1.00×10^{-3}	0.052
1400	0.0	90.4	29.3	100.7	13.9	1.95×10^{-2}	0.256
1400	0.6	57.2	29.3	100.7	13.9	1.95×10^{-2}	0.256

³NB: We found a minus sign missing for the α -N₂ heat of sublimation coefficient A_3 in *Brown and Ziegler's* (1980) Table V, and a spurious discontinuity in their algorithmic fit to the CH₄ heat of sublimation vs. T. We used their source CH₄ data instead (*Ziegler et al.* 1962) to construct Figures 6 and 7. The source data for N₂ are available in *Ziegler and Mullins* (1963).

Table 4							
KBO Atmospheres for Polar Illumination¹							
R (km)	A	r (AU)	T_{crit} (K)	λ	H (km)	Pressure (μbar)	N_{min} (cm-am)
CH₄ (μ=16)							
400	0.0	47.6	40.4	3.41	117	1.03x10 ⁻²	1.29
400	0.6	30.1	40.4	3.41	117	1.04x10 ⁻²	1.29
1400	0.0	37.4	45.6	37.0	37.8	2.91x10 ⁻¹	6.88
1400	0.6	23.7	45.6	37.0	37.8	2.95x10 ⁻¹	6.92
N₂ (μ=28)							
400	0.0	93.3	28.9	8.35	47.9	1.20x10 ⁻²	0.67
400	0.6	59.0	28.9	8.35	47.9	1.21x10 ⁻²	0.67
1400	0.0	75.6	32.1	92.1	15.2	2.62x10 ⁻¹	3.42
1400	0.6	47.8	32.1	92.1	15.2	2.62x10 ⁻¹	3.43

¹In Tables 3 & 4, the ice temperature, column density, and globality pressures given all refer to the minimum required to satisfy the globality constraint discussed in the text; r is the calculated distance beyond which the specified KBO atmospheric case cannot remain global. N_{min} is the resulting corresponding minimum column for globality (for insolation-limited sublimation).

An important caveat to these calculations is that, in the case of sufficiently thin atmospheres or large solar distances, one must take into account that the net sublimation rate of KBO ices is likely to be limited by the one-way sublimation flux, such as would occur into a vacuum. This one-way flux is the maximum at which absorbed insolation can endothermically drive sublimation through supplying the required latent heat. It is proportional to the product of the equilibrium saturation density and mean thermal speed of the gas. Depending on the sticking coefficient and KBO albedo, we find this regime does not occur until 60-80 AU for CH₄ and beyond 100-130 AU for N₂. In this case, it would not be correct to equate the two column abundances above. These distances are large enough that the values in Tables 3 and 4 remain valid.

The structure of a given KBO global atmosphere depends on the ice and atmospheric temperature, KBO radius, and spin orientation. In about half the cases shown in Tables 3 and 4, λ is high enough for the atmosphere to be

“tightly bound” ($\lambda > 25$) though still escaping hydrodynamically. Smaller KBOs with only CH_4 ice can have at best loosely bound atmospheres. The solar distance over which the atmosphere is global then depends on the KBO albedo.

In order to determine the boundary of the regime where globality obtains, we compared the equatorial sublimation wind speed against $0.072v_s$ based on the surface density obtained from the saturation vapor pressure $P_s(T_{\text{ice}})/kT_{\text{ice}}$. Following (Trafton 1984), the equatorial wind speed is:

$$V = 1519\xi[\lambda kT_{\text{ice}}(1-A)(30/r)^2]/[(m_p\mu L(T_{\text{ice}}))P_s(T_{\text{ice}})], \quad (6)$$

where $\xi=0.2812$ for polar insolation and $\xi=0.0289$ for equatorial insolation. T_{ice} is assumed to vary for an ice-covered KBO as $r^{-1/2}$ according to $T_{\text{ice}}=[1.367 \times 10^6(1-A)/(4\sigma r^2)]^{1/4}$. This expresses the radiation balance for a volatile ice covered KBO of arbitrary orientation for which sublimation winds redistribute the solar flux absorbed by the disk evenly over the globe through latent heat transfer, so that the ice isothermally and isotropically radiates this heat to space. As for Tables 3 and 4, T_{ice} in that model is not affected by the orientation of the spin axis relative to the insolation direction. The main difference in the wind speeds for the different insolation geometries arises from the different net sublimation rates. For KBOs with a patchy ice distribution, different values of N could obtain. We neglect ice patchiness here.

Hence, our approach is to begin by assuming such conditions for a KBO atmosphere and then investigating where globality breaks down, e.g., by moving the KBO farther from the Sun. We conservatively neglect ice emissivities less than unity since they would result in higher temperatures and thicker atmospheres.

These equatorial sublimation wind speeds vs. heliocentric distance are compared for various KBO attributes in Figs. 6 and 7 for the equatorial and polar geometries, respectively, for the two plausible ices, CH_4 and N_2 , which differ significantly in volatility. A uniform KBO density of $\rho=1.6 \text{ g cm}^{-3}$ was assumed. KBO atmospheres will be in global hydrostatic equilibrium, with surface pressure varying by less than 10% and volatile ice being nearly isothermal, when they are thick enough that the sublimation wind speed is below the indicated scaled sonic speed. So the hydrostatic regime of the Kuiper belt is the solar distance domain where the curves lie below the

appropriate nearly horizontal curve. Lower than limiting speeds in this regime will give denser global atmospheres; higher ones will not be global.

Figures 6 and 7 show that KBOs with lower albedo and radius can retain global atmospheres and ice isothermality farther away from the Sun than those KBOs with higher albedo or radius, well into the scattered Kuiper belt. This is because the total mass sublimated per unit time is proportional to the disk area of the KBO, while the corresponding sublimation wind mass crossing the equator (or a latitude circle) per unit time is proportional to the product of R , volatile gas column density, and wind speed. Equating these, one sees that the wind speed is directly proportional to R and inversely proportional to the column; hence, small R and large vapor pressure favor subsonic winds and so favor globality.

Also, KBOs with lower axial obliquity can have globally distributed atmospheres deeper into the Kuiper belt. This is because the net diurnally averaged sublimation rate is greater in the high-obliquity configuration of continuous daylight, resulting in faster sublimation winds. Figures 6 and 7 show that KBOs with CH_4 ice would have global atmospheres for solar distances less than 30-50 AU, depending on albedo, size, and obliquity, but KBOs with N_2 ice would have global atmospheres for solar distances less than 45-110 AU, again depending on size, and obliquity.

We emphasize that much larger columns are possible on KBOs than these minimum values for globality. For example, according to Table 3, an $R=400$ km KBO at $r=109$ AU with effectively zero albedo and equatorial illumination having a limiting global N_2 atmosphere will display an ice temperature near 26.7 K, $\lambda=9.0$, $P=1.3 \times 10^{-3}$ μbar , and a critical column $N=0.052$ cm-am. This same KBO at a closer distance to the Sun will exhibit a higher column abundance and its atmosphere will still be global. The speed of the sublimation wind will be less than at $r=109$ AU. This condition is illustrated by the rightmost solid curve on Fig. 6. This curve, as shown, is in the globality regime. Moving down this curve to a solar distance of $r=78$ AU results in an atmosphere with two orders of magnitude lower sublimation wind speed and a correspondingly greater column abundance. Specifically, the solar equilibrium ice temperature will be 31.6 K, $\lambda=7.6$, $P=0.17$ μbar , and the vapor-supported column abundance will be $N=9.6$ cm-am. This is much higher than the column of 0.052 cm-am listed in Table 3 for the limiting wind case.

In summary, KBOs are more likely to exhibit global vs. local atmospheres when the generated sublimation winds are less than 10 m s^{-1} , which corresponds to a volatile gas column abundance at least on the order of 0.05 cm-Am to 7 cm-am. Accordingly, Eqn. (6) implies that higher density and volatility favor globality. And indeed, the limiting atmospheric column abundance for CH_4 globality varies from 0.1 to 7 cm-am for the solar distances listed in Tables 3 and 4, and 0.05 to 3.5 cm-am for N_2 , neglecting ice patchiness. Lower albedo, obliquity, and radius also favor globality, though a low radius also results in a loosely bound atmosphere. Globality is therefore normally restricted to solar distances less than about 55 AU for KBOs with CH_4 ice and less than 120 AU for N_2 ice, depending on the KBO size, albedo, and obliquity. Without a non-solar heat source, such as radioactivity or a transient event, like an impact, a global KBO atmosphere is highly improbable beyond 120 AU.

7. Detection Prospects

As we stated early in this paper, the detection of surface volatiles and high albedos on some KBOs indicates to us that the existence of at least transient (e.g., seasonal) atmospheres on KBOs other than Pluto is highly likely.

Short of sending spacecraft to such KBOs, how might such atmospheres be detected? Stellar occultations observed from Earth are probably the most powerful tools available for the detection of KBOs atmospheres. Although such occultations are capable of detecting atmospheres below microbar pressure levels, stellar occultations of KBOs are rare owing to their tiny angular sizes and slow angular speeds. Moreover, given the fact that astrometric uncertainties for KBO occultations can be substantial, combined with the fact that KBO shadow paths are narrow, makes it necessary to deploy dense grids of observers normal to the occultation path. To capitalize on the rare but valuable KBO occultation events, we urge occultation groups to make event predictions of the kind discussed by *Elliot and Kern* (2003). We further recommend particular emphasis be placed on occultation predictions for large KBOs transiting across dense star fields, such as the galactic center, where occultation event rates are higher than elsewhere on the sky.

A second approach to KBO atmosphere detection is to obtain high-resolution IR spectra to directly search for atmospheric absorptions, as *Young et al.* (1997) did in detecting CH₄ in Pluto's atmosphere. Yet another detection possibility would be to search for faint, extended coma around smaller KBOs which would have atmospheres freely escaping to space. This is the technique that revealed coma around the Centaur Chiron.

In urging observations such as these, we look forward to the day when KBO atmospheres move from the realm of expectation to realization.

Acknowledgements

This work was supported by the New Horizons mission and NASA's Planetary Atmospheres program (Grant NNG04G131G). We thank Mark Bullock, Cathy Olkin, and Jessica Lovering for helpful comments on it. We thank Emmanuel Lellouch and Darrell Strobel for insightful reviews of this manuscript.

References

Barucci, M. A., Cruikshank, D. P., Dotto, E. Merlin, F., Poulet, F., Dalle Ore, C., Fornasier, S., and de Bergh, C. (2005) Is Sedna Another Triton? *Astron. Astrophys.*, 439, L1-L4.

Brosch, N. (1995). The 1985 Stellar Occultation by Pluto. *MNRAS*, 276, 571-575.

Brown G. N., and Ziegler W. T. (1980) Vapor Pressure and Heats of Sublimation of Liquids and Solids of Interest in Cryogenics Below 1-atm Pressure. In *Advances in Cryogenic Engineering*, 25, eds. K. Timmerhaus and H. A. Snyder (New York: Plenum Press), pp. 662-670.

Bus S. J., A'Hearn M. F., Schleicher D. G., and Bowell E. (1991) Detection of CN emission from (2060) Chiron. *Science* 251, 774-777.

Bus, S.J., A'Hearn M.F., Bowell, E. and Stern S.A. (1991) Chiron: Evidence for Historic Activity. *LPSC, XXIII*, p. 34.

Capria M. T., Coradini A., De Sanctis M. C., and Orosei R. (2000) Chiron Activity and Thermal Evolution. *Astronomical Journal* 119, 3112-3118.

Choi Y., Cohen M., Merk R., Prialnik D. (2002) Long-Term Evolution of Objects in the Kuiper Belt Zone-Effects of Insolation and Radiogenic Heating. *Icarus*, 160, 300-312.

Cruikshank D. P., Pilcher C. B., and Morrison D. (1976) Pluto—Evidence for methane frost. *Science* 194, 835-837. Doute S., Schmitt B., Quirico E., Owen T., Cruikshank D., deBergh C., Geballe T., and Roush T. (1999), Evidence for Methane Segregation at the Surface of Pluto. *Icarus* 142, 421-444.

Durda D. D., Stern S. A. (2000) Collision Rates in the Present-Day Kuiper belt and Centaur Regions: Applications to Surface Activation and Modification on Comets, Kuiper Belt Objects, Centaurs and Pluto-Charon. *Icarus*, 145, 220-229.

Elliot J. L., Dunham E. W., Bosh A. S., Slivan S. M., Young L. A., Wasserman L. H., and Millis R. L. (1989) Pluto's atmosphere. *Icarus*, 77, 148-170.

Elliot J. L., Olkin C. B., Dunham E. W., Ford C. H., Gilmore D. K., Kurtz D., Lazzaro D., Rank D. M., Temi P., Bandyopadhyay R. M., Barroso J., Barrucci A., Bosh A. S., Buie M. W., Bus S. J., Dahn C. C., Foryta D. W., Hubbard W. B., Lopes D. F., and Marcialis R. L. (1995) Jet-Like Features Near the Nucleus of Chiron. *Nature*, 373, 46-46.

Elliot, J. L., Strobel, D. F., Zhu, X., Stansberry, J. A., Wasserman, L. H., and Franz, O. G. (2000) The Thermal Structure of Triton's Middle Atmosphere. *Icarus*, 143, 425-428.

Elliot J. L., and Kern S. D. (2003) Probing Large KBOs for Atmospheres and Companions. 35th DPS Meeting, 35.44.

Elliot J. L., Ates A., Babcock B. A., Bosh A. S., Buie M. W., Clancy K. B., Dunham E. W., Eikenberry S. S., Hall D. T., Kern S. D., Leggett S. K., Levine S. E., Moon D.-S., Olkin C. B., Osip D. J., Pasachoff J. M., Penprase B. E., Person M. J., Qu S., Rayner J. T., Roberts L. C., Salyk C. V., Souza S. P., Stone R. C., Taylor B. W., Tholen D. J., Thomas-Osip J. E., Ticehurst D. R., and Wasserman L. H. (2003) The recent expansion of Pluto's atmosphere. *Nature*, 424, 165-168.

Eshelman V. R. (1989) Pluto's Atmosphere: Models Based on Refraction, Inversion, and Vapor-Pressure Equilibrium. *Icarus*, 80, 439-443.

Grundy W. M., and Buie M. W. (2000) The Distribution and Physical State of H₂O on Charon. *Icarus*, 148, 324-339.

Hart M. H. (1974) A Possible Atmosphere for Pluto. *Icarus*, 21, 242-247.

Hainaut O. R., Delahodde C. E., Boehnhardt H., Dotto E., Barucci M. A., Meech K. J., Bauer J. M., West R. M., and Doressoundiram A. (2000) Physical Properties of TNO 1996 TO66. Light Curves and Possible Cometary Activity. *Astronomy and Astrophysics* 356, 1076-1088.

Hansen C. J. and Paige D. A. (1996) Seasonal Nitrogen Cycles on Pluto. *Icarus* 120, 247-265.

Hartmann W. K., Tholen D. J., Meech K. J., and Cruikshank D. P. (1990) 2060 Chiron—Colorimetry and Cometary Behavior. *Icarus* 83, 1-15.

Hubbard W. B., Hunten D. M., Dieters S. W., Hill K. M., and Watson R. D. (1988) Occultation Evidence for an Atmosphere on Pluto. *Nature* 336, 452-454.

Hubbard W. B., Yelle R. V., and Lunine J. I. (1990) Non-Isothermal Pluto Atmosphere Models. *Icarus*, 84, 1-11.

Hunten D. M., and Watson A. J. (1982) Stability of Pluto's Atmosphere. *Icarus*, 51, 665-667.

Ingersoll A. P. (1990) Dynamics of Triton's Atmosphere. *Nature*, 344, 315-317.

Jewitt D. C. (1994) Heat from Pluto. *Astronomical Journal*, 107, 372-378.

Jewitt D. C. and Luu J. (2004) Crystalline Water Ice on the Kuiper Belt Object (50000) Quaoar. *Nature*, 432, 731-733.

Krasnopolsky, V. A. (1993) On the Haze model for Triton. *JGR* 98, 17123-17124

Krasnopolsky, V. A. (1999) Hydrodynamic Flow of N₂ from Pluto. *JGR*, 104, 5955-5962.

Lellouch, E., Laureijs, R., Schmitt, B., Quirico, E., de Bergh, C., Crovisier, J., and Coustenis, A. (2000) Pluto's Non-isothermal Surface. *Icarus*, 147, 220-250.

Licandro J., Pinilla-Alonso N., Pedani M., Oliva E., Tozzi G. P., and Grundy W. M. (2006) The Methane Ice Rich Surface of Large TNO 2005 FY9: A Pluto-Twin in the Trans-Neptunian Belt? *Astronomy and Astrophysics*, 445, L35-L38.

Lykawka P. S., and Mukai T. (2005) Higher Albedos and Size Distribution of Large Transneptunian Objects. *Planetary and Space Science*, 53, 1319-1330.

McKinnon W. B. (2002) On the Initial Thermal Evolution of Kuiper Belt Objects. In: Proceedings of Asteroids, Comets, Meteors—ACM (2002) International Conference, 29 July—2 August 2002, Berlin, Germany. Ed. Barbara Warmbein. ESA SP-500. Noordwijk, Netherlands: ESA Publications Division, ISBN 92-9092-810-7, p. 29-38.

McNutt R. L. (1989) Models of Pluto's Upper Atmosphere. *GRL.*, *16*, 1225-1228.

Meech K. J. and Belton M. J. S. (1989) (2060) Chiron. *International Astronomical Union Circular 4770*, 1.

Orosei R., Coradini A., de Sanctis M. C., and Federico C. (2001) Collision-induced thermal evolution of a comet nucleus in the Edgeworth-Kuiper Belt. *Advances in Space Research 28*, 1563-1569.

Owen T. C., Roush T. L., Cruikshank D. P., Elliot J. L., Young L. A., de Bergh C., Schmitt B., Geballe T. R., Brown R. H., and Bartholomew M. J. (1993) Surface Ices and the Atmospheric Composition of Pluto. *Science*, *261*, 745-748.

Pasachoff J. M., Souza S. P., Babcock B. A., Ticehurst D. R., Elliot J. L., Person M. J., Clancy K. B., Roberts L. C., Hall D. T., and Tholen D. J. (2005) The Structure of Pluto's Atmosphere from the 2002 August 21 Stellar Occultation. *Astronomical Journal*, *129*, 1718-1723.

Sicardy B., Widemann T., Lellouch E., Veillet C., Cuillandre J.-C., Colas F., Roques F., Beisker W., Kretlow M., Lagrange A.-M., Gendron E., Lacombe F., Lecacheux J., Birnbaum C., Fienga A., Leyrat C., Maury A., Raynaud E., Renner S., Schultheis M., Brooks K., Delsanti A., Hainaut O. R., Gilmozzi R., Lidman C., Spyromilio J., Rapaport M., Rosenzweig P., Naranjo O., Porras L., Dandiacute;az F., Calderón H., Carrillo S., Carvajal A., Recalde E., Cavero L. G., Montalvo C., Barría D., Campos R., Duffard R., and Levato H. (2003) Large Changes in Pluto's Atmosphere as Revealed by Recent Stellar Occultations. *Nature*, *424*, 168-170.

Sicardy, B., Bellucci, A., Gendron, E., Lacombe, F., Lacour, S., Lecacheux, J., Lellouch, E., Renner, S., Pau, S., Roques, F., and 35 others (2006)

Charon's Size and an Upper Limit on its Atmosphere from a Stellar Occultation. *Nature*, 439, 52-54.

Spencer J. R., Stansberry J. A., Trafton L. M., Young E. F., Binzel R. P., and Croft S. K. (1997) Volatile Transport, Seasonal Cycles, and Atmospheric Dynamics on Pluto. In *Pluto and Charon*, edited by S. A. Stern and D. J. Tholen. Tucson: University of Arizona Press, 435-473.

Stansberry J. A., Lunine J. I., Hubbard W. B., Yelle R. V., and Hunten D. M. (1994) Mirages and the Nature of Pluto's Atmosphere. *Icarus*, 111, 503-513.

Stern S. A. (1981) Theoretical Investigations of the Atmospheric Environment of Pluto. S. A. Stern, Masters Thesis, University of Texas, 1981.

Stern S. A. (1989) Pluto-Comments on Crustal Composition, Evidence for Global Differentiation. *Icarus*, 81, 14-23.

Stern S. A. (1999) The Lunar Atmosphere. *Space Sci. Reviews*, 37, 453-520.

Stern S. A., and Trafton L. (1984) Constraints on bulk composition, seasonal variation, and global dynamics of Pluto's atmosphere. *Icarus*, 57, 231-240.

Stern S. A., Trafton L., and Gladstone G. (1988) Why is Pluto bright? Implications of the albedo and lightcurve behavior of Pluto. *Icarus*, 75, 485-498.

Stern S. A., Weintraub D. A., and Festou M. C. (1993) Evidence for a Low Surface Temperature on Pluto from Millimeter-Wave Thermal Emission Measurements. *Science*, 261, 1713.

Strobel D. F., Zhu X., Summers M. E., and Stevens M. H. (1996) On the Vertical Thermal Structure of Pluto's Atmosphere. *Icarus*, 120, 266-289.

Summers, M. E., and Strobel, D. F. (1991) Triton's Atmosphere—A Source of N and H for Neptune's Magnetosphere. *GRL*, 18, 2309-2312.

Tian, F., and Toon, O. B. (2005) Hydrodynamic Escape of Nitrogen from Pluto. *GRL* 32, L18201.

Trafton L., and Stern S. A. (1983) On the Global Distribution of Pluto's Atmosphere. *Astrophysical Journal*, 267, 872-881.

Trafton L. (1984) Large Seasonal Variations in Triton's Atmosphere. *Icarus*, 58, 312-324.

Trafton L. M., Whipple, A. L., and Stern S. A. (1989) Hydrodynamic Calculations of Pluto's Atmosphere. *Ninth Planet News* 7, 1-2.

Trafton L. (1990) A two-component Volatile Atmosphere for Pluto. I—The Bulk Hydrodynamic Escape Regime. *Astrophysical Journal*, 329, 512-523.

Trafton L. M., and Stern S. A. (1996) Rotationally Resolved Spectral Studies of Pluto from 2500 to 4800 Å Obtained from HST. *Astronomical Journal*, 112, 1212-1224.

Trafton L. M., Hunten D. M., Zahnle K. J., McNutt R. L., Jr. (1997) Escape Processes at Pluto and Charon. In: *Pluto and Charon*, edited by S. A. Stern and D. J. Tholen. Tucson: University of Arizona Press, 475-522.

Womack M., and Stern S. A. (1999) Detection of Carbon Monoxide in (2060) Chiron. *Solar System Research (Astronomicheskii Vestnik)*, 33, 187-192.

Yelle R. V., Elliot J. L. (1997) Atmospheric Structure and Composition: Pluto and Charon. In *Pluto and Charon*, edited by S. A. Stern and D. J. Tholen. Tucson: University of Arizona Press, 347-390.

Yelle R. V. and Lunine J. I. (1989) Evidence for a Molecule Heavier than Methane in the Atmosphere of Pluto. *Nature*, 339, 288-290.

Yelle R. V. (1993) Hydrodynamic Escape of Pluto's Atmosphere. Presented at the *Pluto & Charon* meeting, July 6-9, 1993 in Flagstaff, AZ. Abstract booklet p. 74.

Young L. A., Elliot J. L., Tokunaga A., de Bergh C., and Owen T. (1997) Detection of Gaseous Methane on Pluto. *Icarus*, 127, 258-270.

Ziegler, W. T., Mullins, J. C., and Kirk, B. S. (1962) Calculation of the Vapor Pressure and Heats of Vaporization and Sublimation of Liquids and

Solids, Especially Below One Atmosphere, III. Methane. Tech. Report No. 3, Project No. A-460, Engineering Experiment Station, Georgia Institute of Technology, August 31, 1962 (Contract No. CST-7238, National Bureau of Standards, Boulder, Colorado).

Ziegler, W. T., and Mullins, J. C. (1963) Calculation of the Vapor Pressure and Heats of Vaporization and Sublimation of Liquids and Solids, Especially Below One Atmosphere, IV. Nitrogen and Fluorine. Tech. Report No. 1, Project No. A-663, Engineering Experiment Station, Georgia Institute of Technology, April 15, 1963 (Contract No. CST-7404, National Bureau of Standards, Boulder, Colorado). (See also, "Corrections to Nitrogen and Fluorine Report", minor corrections to this report issued July 2, 1963.)

Figure Captions

Figure 1. Data (points; *Elliot et al.*, 1989) and model (line; *Elliot and Young*, 1992) resulting from a KAO light curve from Pluto's 1988 stellar occultation. The points along the bottom are the residuals that result when the model and the data are differenced.

Figure 2. Surface and vapor pressures on Pluto (*Young et al.*, 1997). The upper curve for N₂ should be close to the total atmospheric surface pressure, and the lower curve for CH₄ is for the same mixture as for the N₂, where as the middle curve is for pure CH₄. The solid parts of the curves show the vapor pressures for a frost temperature of 40±2 K.

Figure 3. Pluto's vertical thermal structure and thermal gradient as retrieved from the 2002 stellar occultation (from *Sicardy et al.* 2003).

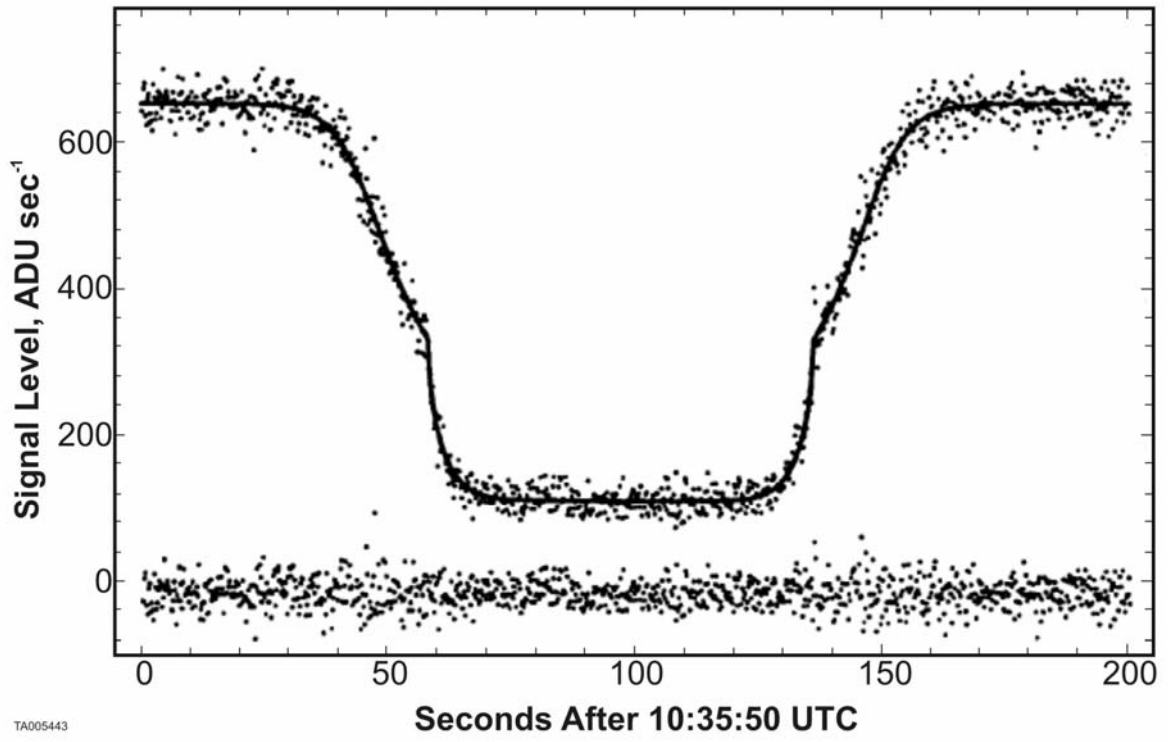
Figure 4. Equilibrium vapor pressure curves for CH₄, CO, and N₂ as a function of temperature.

Figure 5. Pressure vs. altitude curves for simple, isothermal atmospheres for KBOs with various sizes and surface temperatures with pure N₂ and CH₄ atmospheres. Panel (a) T=50 K. Panel (b) T=30 K. The solid curves refer to a radius of R=1400 km, and the dashed curves to R=400 km. The heavier curves refer to N₂ and the lighter ones to CH₄. A surface pressure of 15 microbars and a KBO density of 1.6 g cm⁻³ are assumed.

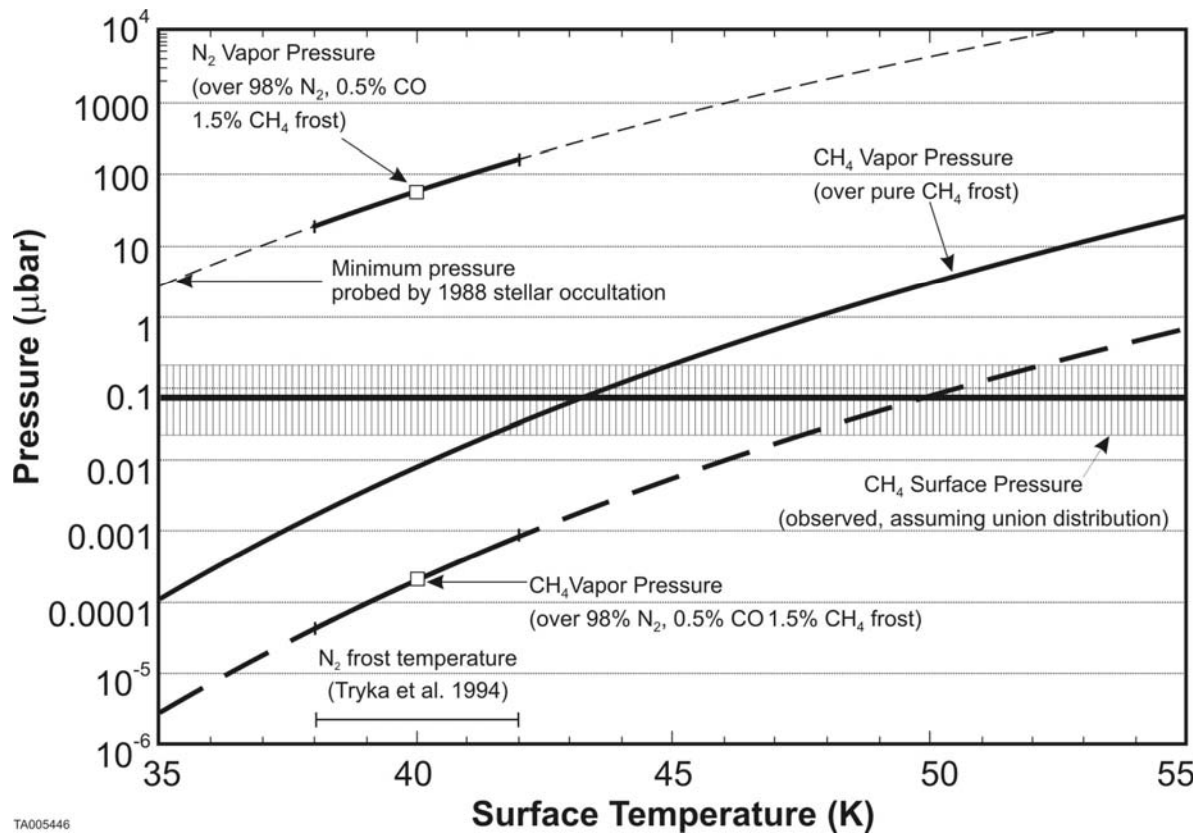
Figure 6. Hemispherical sublimation wind speeds in KBO atmospheres for subsolar latitude 0 deg vs. solar distance. Curves are shown for KBO albedo A and KBO radius R of two gases of very different volatility. The four curves on the left are for CH₄ and the four on the right are for N₂. The heavy curves are plotted for albedo A=0 and the dashed ones for A=0.6. The upper (or leftmost) curve for each iso-albedo pair is for R=1400 km and the lower (or rightmost) is for R= 400 km. The nearly horizontal curves indicate 7.2% of the speed of sound for atmospheric N₂ (solid) and CH₄ (dot-dash). KBO atmospheres will be in global hydrostatic equilibrium, with surface pressure varying by less than 10% and volatile ice being nearly isothermal, when they are thick enough (see Tables 3 and 4) that the sublimation wind speed is below the indicated scaled sonic speed. Rapidly rotating, volatile-ice

covered, spherical KBOs are assumed at the radiative balance temperature; and atmospheric escape is neglected.

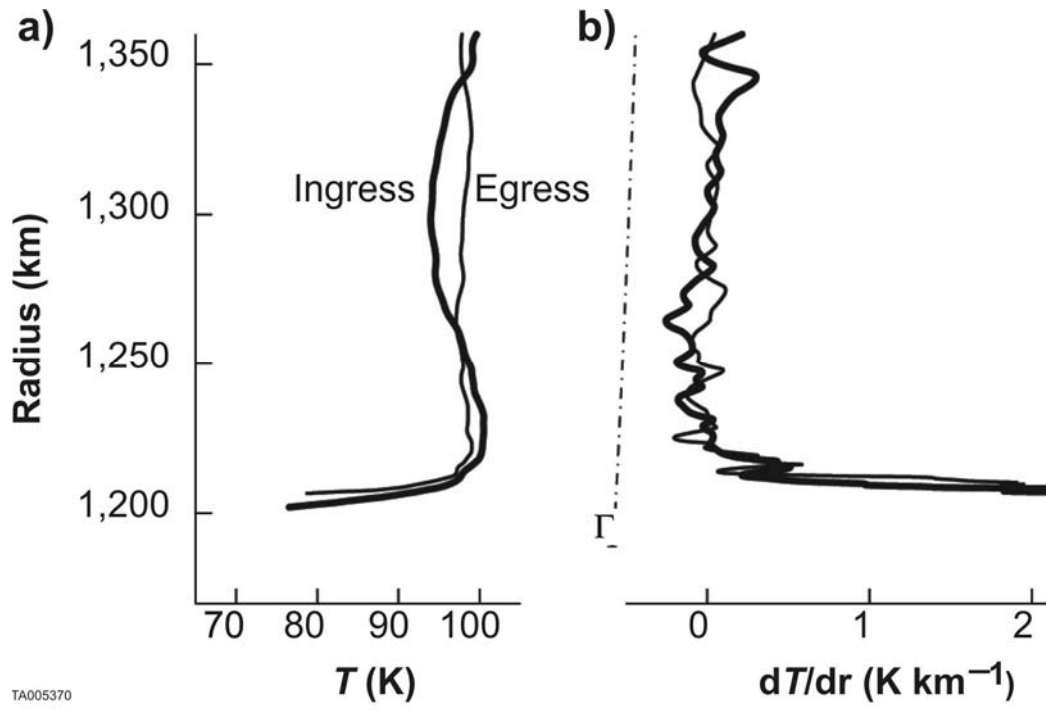
Figure 7. Same as Fig. 6 for subsolar latitude 90 deg without regard to rotation rate. KBOs with high obliquity are less likely to have globally distributed atmospheres deep into the Kuiper belt than low obliquity KBOs.



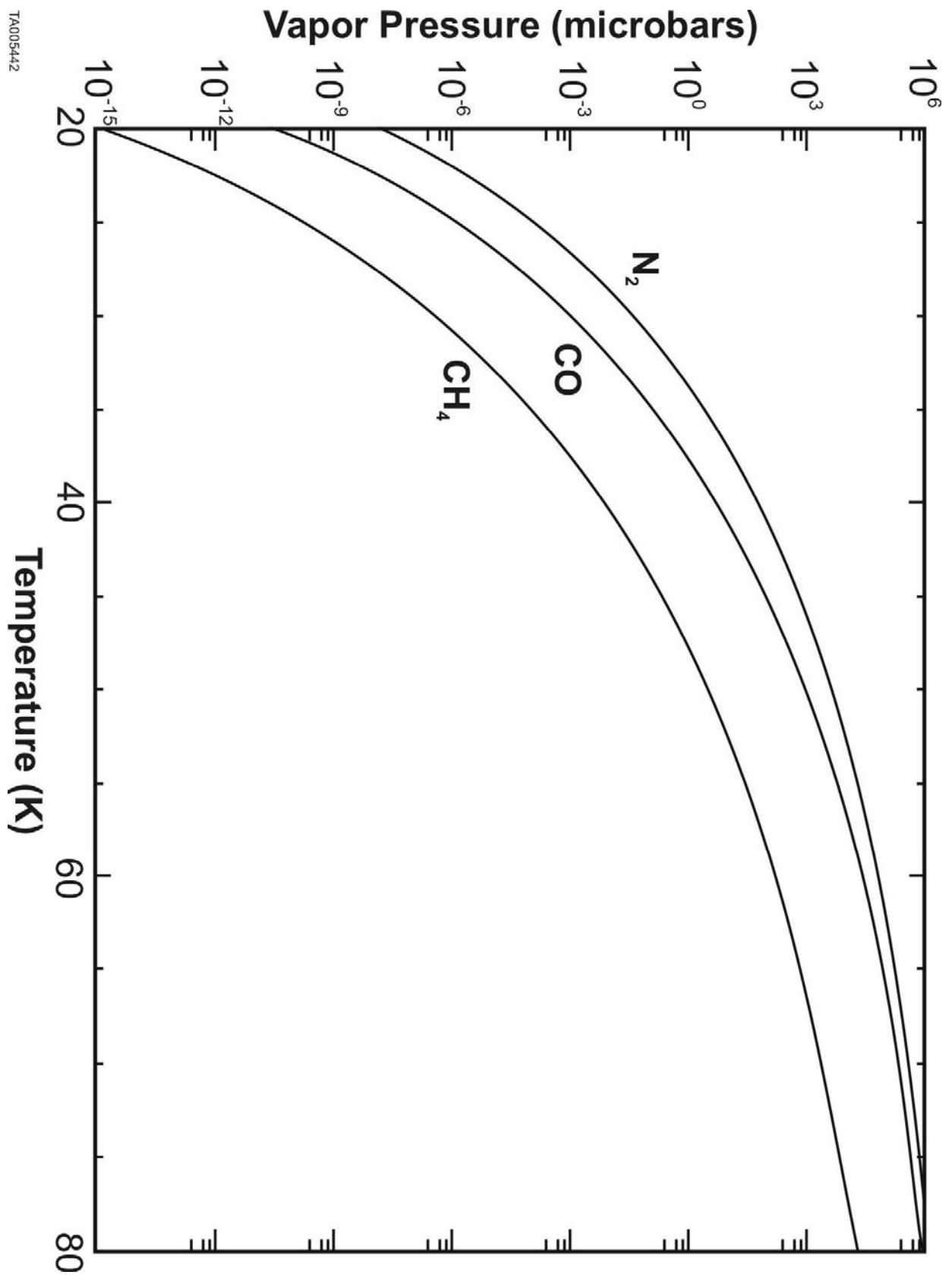
TA005443

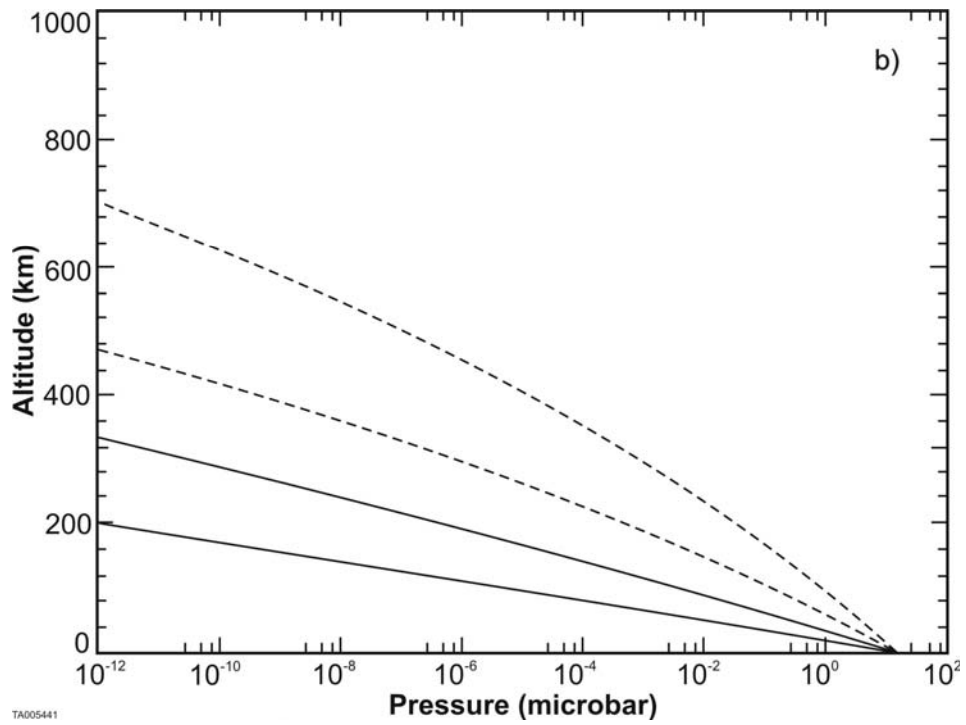
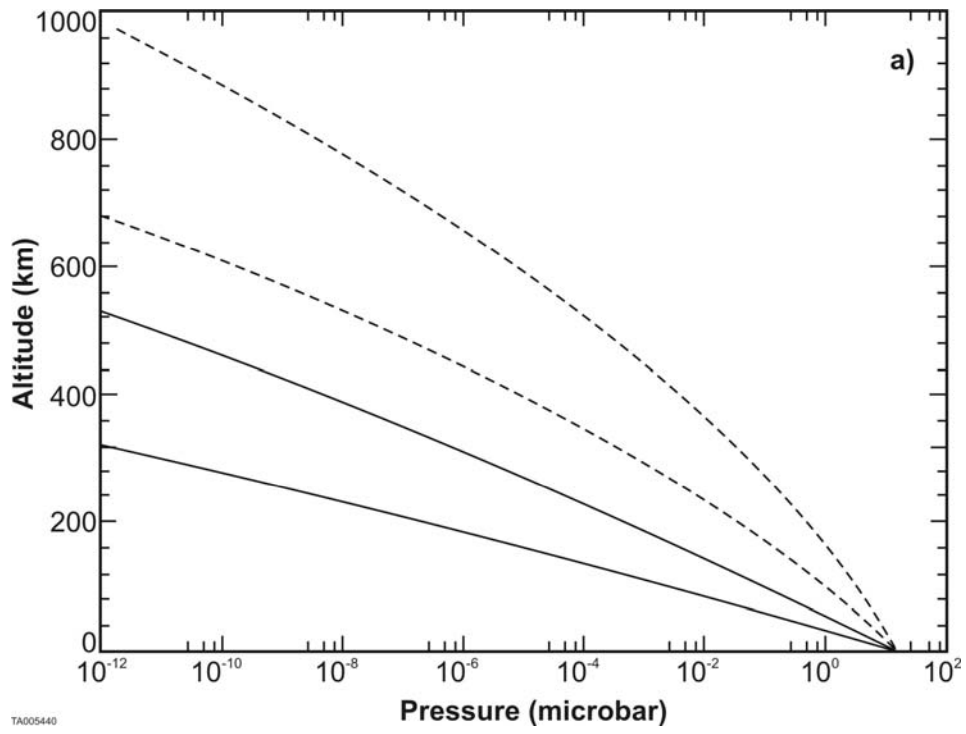


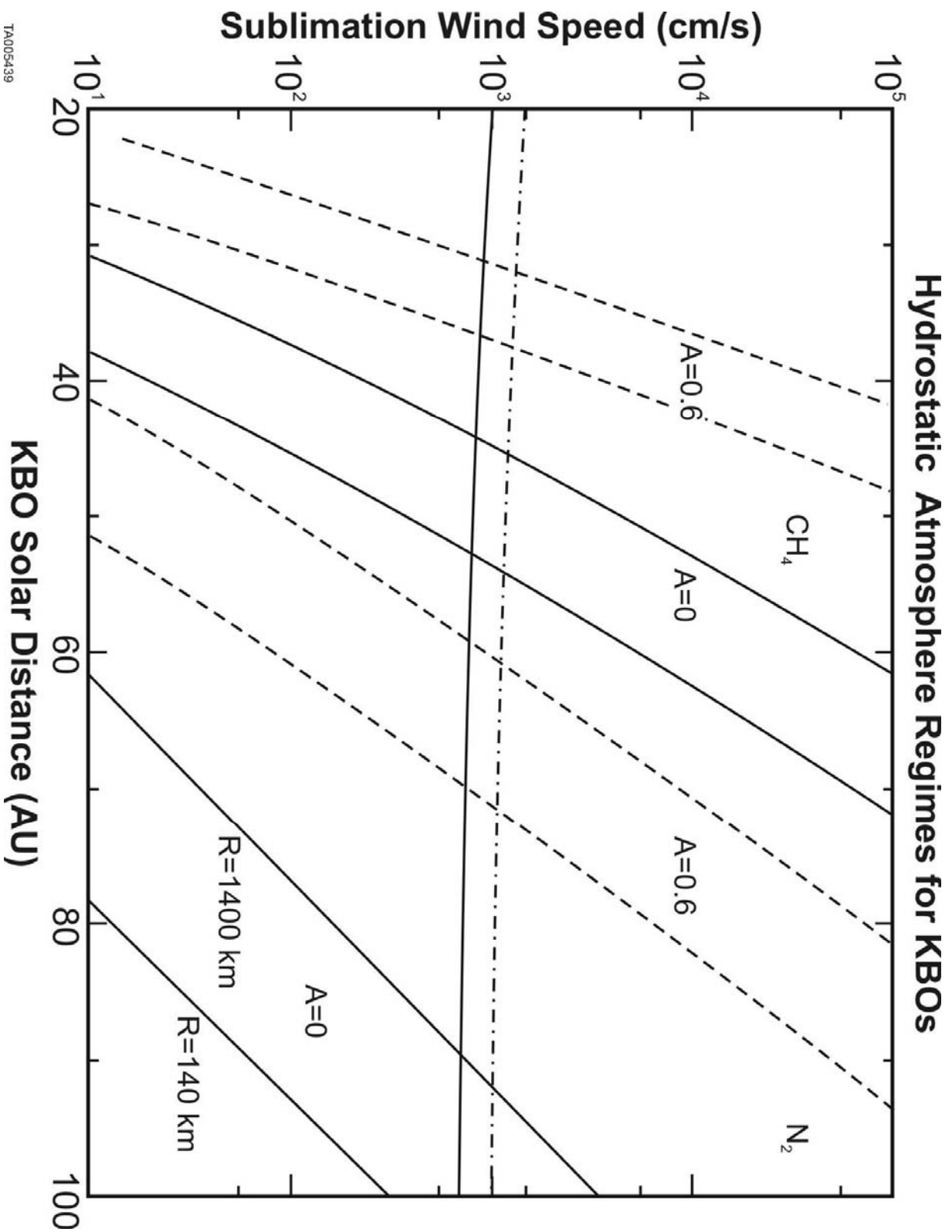
TA005446

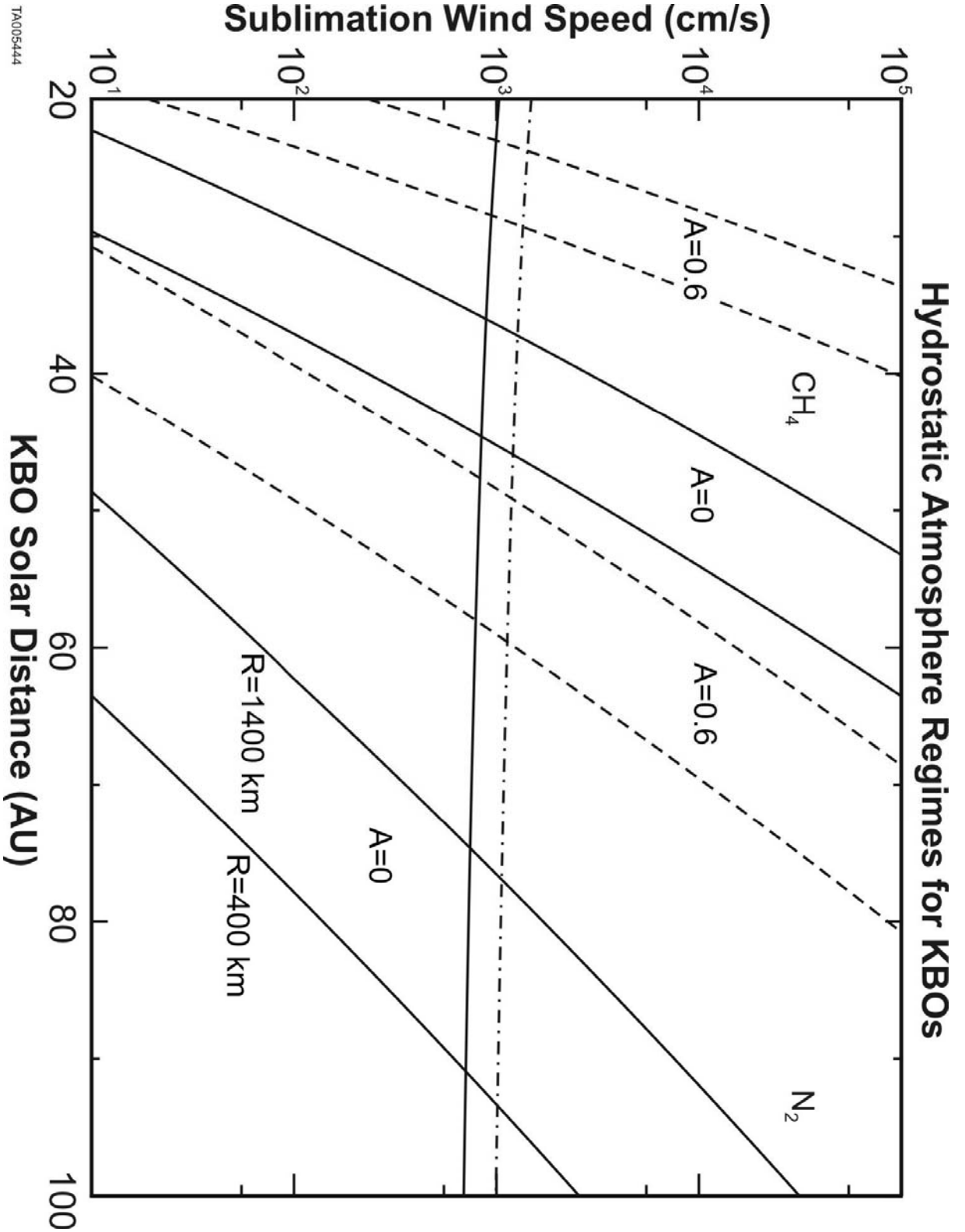


TA005370









TA005444